Journal of Power Sources 196 (2011) 1508–1512

Contents lists available at ScienceDirect

Journal of Power Sources

journal homepage: www.elsevier.com/locate/jpowsour

Short communication

Surface potential measurement of aged Li-ion batteries using Kelvin probe microscopy

Shrikant C. Nagpure [a], Bharat Bhushan [a,*], S.S. Babu [b]

[a] Nanoprobe Laboratory for Bio-& Nanotechnology and Biomimetics (NLBB), Ohio State University, Columbus, OH 43212, United States
[b] Material Science and Engineering, Ohio State University, Columbus, OH 43212, United States

ARTICLE INFO

Article history:
Received 23 June 2010
Received in revised form 4 August 2010
Accepted 5 August 2010
Available online 18 August 2010

Keywords:
Batteries
Energy storage
Aging
Atomic force microscope (AFM)
Electric vehicles (EV)
Kelvin probe microscopy (KPM)

ABSTRACT

In lithium-ion batteries, several electrical and physical parameters are responsible for the degradation of the electrode materials. Here the application of Kelvin probe microscopy (KPM) is demonstrated to measure the charge sustaining capability of the $LiFePO_4$ cathode under aged and unaged conditions. The aged sample shows lower surface potential than the unaged sample, which can be attributed to changes in physical and chemical properties including particle size, phase of the surface layer and nanocrystalline deposits.

1. Introduction

Advanced Li-ion batteries with high energy and power density are favored for automotive demands. While the operation of the Li-ion cell is well established, the aging mechanisms still need to be investigated as the aging of a Li-ion battery is still the weak link in the development of long lasting hybrid vehicles [9]. The harsh duty cycles (high current demand, low state of charge, deep depth of discharge, and high temperature profiles) in hybrid/electric vehicles cause the loss of capacity (range) and power (performance) in the battery system faster than normal rate. The degradation or "aging" is a result of several simultaneous physiochemical processes that occur within the electrode, electrode–electrolyte interface, and within the electrolyte.

The aging of a battery causes a decrease in capacity and a subsequent increase in the internal resistance. The degradation in these system level parameters is due to damage in the cathode, anode, and electrolyte within the cell. The surface electrical properties need to be evaluated for a better understanding of the damage mechanisms of the electrodes. Surface resistance properties have been measured for $LiFePO_4$ unaged and aged cathodes using scanning spreading resistance microscopy (SSRM) [10].

Another technique of interest is KPM, which has been used in a variety of applications to measure surface potential. Because of the sensitive nature of silicon to charge buildup and subsequent discharge which can damage small silicon parts, surface potential measurement has been of interest in the semiconductor industry. The technique has also been used successfully to detect wear precursors from wear at very low loads using atomic force microscopy (AFM) based Kelvin probe methods [5–7].

The use of the Kelvin probe method is now extended to the study of Li-ion batteries. The KPM technique is based on the contact potential difference method for measuring the electronic work function (EWF) [14]. Since EWF is strongly influenced by the surface chemical composition and Fermi level of the material KPM can detect the structural and chemical changes of the surface and provide vital information about the onset of damage. Using KPM large areas of the entire cathode electrode can be scanned quickly giving spatial information of its surface. In this study, KPM is used for the first time to characterize aging of the cathode surfaces by measuring the change in the surface potential which can be attributed to physical and chemical changes of surface.

2. Experimental details

2.1. Kelvin probe microscopy

Nanoscale surface potential measurements were taken with a Dimension™ 3100 AFM. A schematic of this instrument with KPM setup is shown in Fig. 1. The KPM measures the surface poten-

* Corresponding author at: The Ohio State University, Nanoprobe Laboratory for Bio- & Nanotechnology and Biomimetics, 201 West 19th Avenue, Columbus, OH 43210-1142, United States. Tel.: +1 614 292 0651; fax: +1 614 292 0325.
E-mail address: bhushan.2@osu.edu (B. Bhushan).

0378-7753/$ – see front matter © 2010 Elsevier B.V. All rights reserved.
doi:10.1016/j.jpowsour.2010.08.031

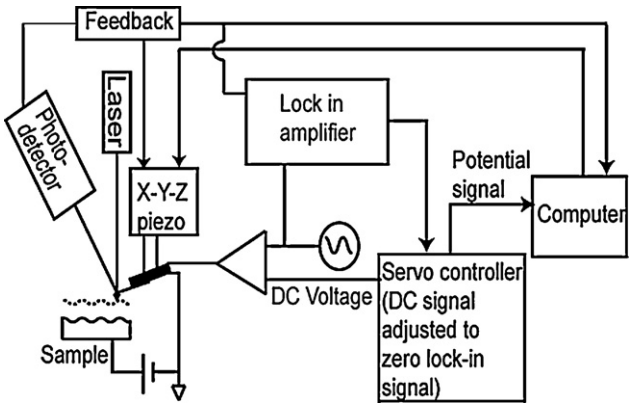

Fig. 1. Schematic of the two pass interleave scan method used in KPM. (Adapted from Rice, 2002 [12].)

tial of the samples in interleave mode. Along one scan line on the sample, in first pass, the surface height image is obtained in tapping mode. In second pass the tip is lifted off the sample surface and a surface potential map is obtained. Both images are obtained simultaneously [12]. During the first pass, the cantilever is mechanically vibrated by the *X–Y–Z* piezo near its resonance frequency. The amplitude of the tip vibrations (not shown) is maintained at a constant value by the feedback loop as the tip scans the surface of the sample. The signal from the feedback loop is used to construct the height map of the sample surface (Fig. 1). During the interleaved scan, the *X–Y–Z* piezo is switched off. Instead, an AC signal is applied directly to the conductive tip which generates an oscillating electrostatic force on the tip. The tip is scanned along the surface topography line obtained in the tapping mode with a certain lift off the sample (dotted line in Fig. 1).

To briefly describe the operating principle of KPM, consider a tip and sample interaction as seen in Fig. 2. When the tip and sample are electrically connected (Fig. 2a) electrons flow from the material with the lower work function to the material with the higher work function. Due to the difference in the work function of the electrically connected tip and the sample an electrostatic contact potential difference (or surface potential difference) is created between the tip and the sample [14]. The value of this surface potential ($\Delta\Phi$) is given by the following equation:

$$\Delta\Phi = \frac{\Phi_{tip} - \Phi_{sample}}{e} \tag{1}$$

where Φ_{tip} and Φ_{sample} are work functions of the tip and the sample, respectively, and e is the magnitude of the charge of one electron. $\Delta\Phi$ will be affected by any adsorption layer and the phase of the material near the surface. Electrostatic force is created between the tip and sample under the influence of this surface potential difference and the separation dependent local capacitance C of the tip and sample. This force is given by:

$$F = \frac{1}{2}(\Delta\Phi)^2 \frac{\partial C}{\partial z} \tag{2}$$

where z is the distance between the tip and sample.

Along with $\Delta\Phi$, in the operation of the KPM a compensating DC voltage signal (V_{DC}) and AC voltage signal, $V_{AC}\sin(\omega t)$ (Fig. 2b and c) is applied directly to the tip. Thus the electrostatic force between the tip and the sample becomes:

$$F = \underbrace{\frac{1}{2}\frac{\partial C}{\partial z}\left\{(\Delta\Phi + V_{DC})^2 + \frac{V_{AC}^2}{2}\right\}}_{\text{DC-term}} + \underbrace{\frac{\partial C}{\partial z}(\Delta\Phi + V_{DC})V_{AC}\sin(\omega t)}_{\omega\text{-term}}$$

$$- \underbrace{\frac{1}{4}\frac{\partial C}{\partial z}V_{AC}^2\cos(2\omega t)}_{2\omega\text{-term}} \tag{3}$$

The cantilever responds only to the forces at or very near its resonance frequency. Thus, only the oscillating electric force at ω acts as a sinusoidal driving force that can excite oscillations in the cantilever. The DC and the 2ω terms do not cause any significant oscillations of the cantilever. In tapping mode, the cantilever response (RMS amplitude) is directly proportional to the drive amplitude of the tapping piezo. Here, in the interleave mode the response is directly proportional to the amplitude of the ω term [12]. The servo controller applies a DC voltage signal equal and out of phase with $\Delta\Phi$ so that the amplitude of the tip becomes zero ($F = 0$). This compensating signal from the servo controller creates the surface potential map of the sample [6].

The conductive AFM tip is necessary for the KPM experiments. The tips used in our experiments had an electrically conductive 5-nm-thick chromium coating and 25-nm-thick platinum coating on both sides of the cantilever (Budget Sensors, Model # Multi75E-G). The resonant frequency of the tips was 75 kHz, and the radius was less than 25 nm. The interleave height was optimized to 150 nm for a good surface potential signal.

2.2. Demonstration sample

The operation of the KPM technique is demonstrated with a sample shown in Fig. 3a. A single crystal silicon (1 0 0) wafer with a high resistivity of about 3.3 kΩ cm is chosen as a substrate. A SiO_2 layer of about 200 nm is grown on the substrate with thermal oxidation process. Then, using an evaporation process two distinct rectangular pads of Ti/Au with a separation distance of 15 μm are deposited on the sample. The thickness of the Ti coating is about 50 nm, and the thickness of the Au coating is about 200 nm. Electrical connections are made to the pads using micro-probes available from Accuprobe™.

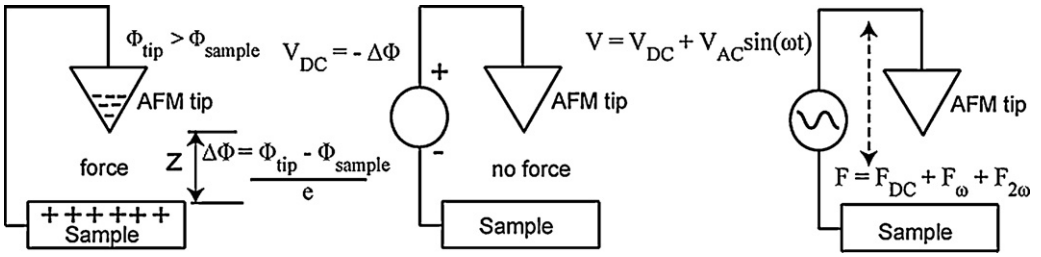

Fig. 2. (a) Electrostatic potential and interaction force between a conducting tip and a sample (for illustration $\Phi_{tip} > \Phi_{sample}$ is assumed), (b) external DC voltage applied to nullify the force, and (c) external AC voltage with adjustable DC offset is applied to the tip which leads to its vibration. (Adapted from Bhushan and Goldade, 2000 [6].)

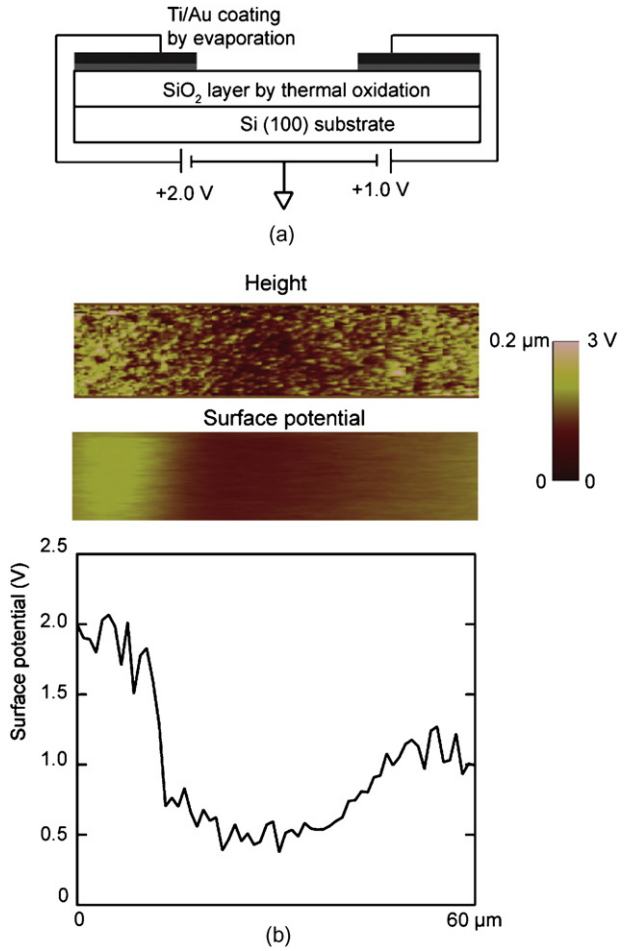

Fig. 3. (a) Schematic of the demonstration sample and (b) surface height and surface potential maps, and a profile of the surface potential map obtained by averaging over multiple scan lines.

2.3. Li-ion battery samples

Two identical cylindrical type Li-ion batteries were chosen for the experiments to prepare unaged and aged $LiFePO_4$ cathode samples. The anode in the batteries is made of graphite bonded onto a copper substrate. The cathode is made of $LiFePO_4$ nanoparticles (diameter between 40 and 50 nm) bonded onto an aluminum substrate using a polyvinylidene difluoride binder. To improve the poor conductivity (2×10^{-9} S cm^{-1}) [4] of $LiFePO_4$ nanoparticles, these are coated with carbon [8]. An alternating stack of separator, anode, separator, and cathode is rolled and packed into a cylindrical aluminum casing. The casing is then filled with an electrolyte made of hexafluorophosphate ($LiPF_6$) salt dissolved in alkylene carbonates.

The cell had an operating voltage of 3.3 V and a nominal discharge capacity of 2.3 Ah. One battery was charged and discharged completely at 1 C (1 C = 2.3 Ah) rate to verify its rated capacity. This battery was labeled as an unaged battery. The other battery was cycled at 45 °C with a 16 C rate at 50% state of charge and ±5% depth of discharge until the capacity dropped by 20%. This battery was labeled as an aged battery. According to the automobile industry, a battery is said to have reached its end of life (EOL) if the capacity degrades by 20% of its original capacity [1]. It took 33,600 cycles for the aged battery to reach EOL.

The unaged and aged batteries were discharged completely after being cycled for the required number of cycles. The batteries were then disassembled in air, and the long cathode strip (1525 mm × 65 mm) was acquired. The samples for this study were then cut from this long strip, from the area closer to the center of the battery, and care was taken to cut samples from approximately the same area from the unaged and aged battery.

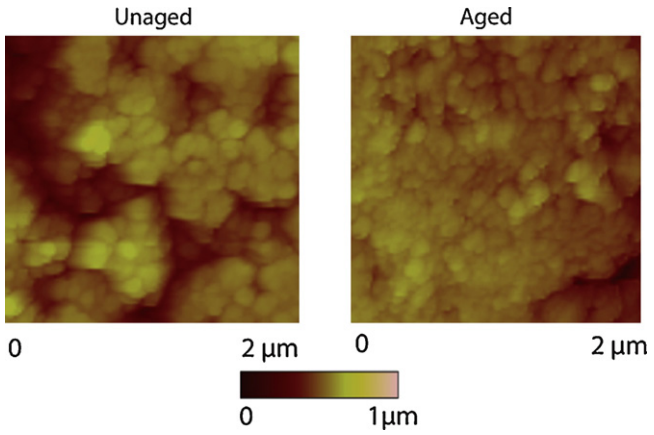

Fig. 4. Surface height image of the unaged and the aged $LiFePO_4$ cathode samples. Coarsening of the nanoparticles is observed in the aged surface height map.

3. Results and discussion

3.1. Demonstration sample

The demonstration sample was mounted on a non-conductive double sided tape. A +2.0 and +1.0 V potential was directly applied to the right and left pad, respectively, from an external DC power source. Both the pads had a common ground. The two distinct Ti/Au pads with a separation distance of 15 μm are visible in the surface height image shown in Fig. 3b. The contrast in the surface potential measured over the two Ti/Au pads can be observed in Fig. 3b. A profile of the surface potential map is also shown in the Fig. 3b. This profile was obtained by averaging the surface potential values obtained over multiple scan lines. The right pad is at about +2.0 V. The surface potential value starts to drop as the tip approaches the valley between the two pads. The potential value drops to minimum as the tip scans over the 15 μm separation distance. The potential value rises again to +1.0 V as the tip scans over the left pad. This measurement demonstrated the validity and accuracy of the KPM technique using Dimension™ 3100 AFM.

3.2. Unaged and aged $LiFePO_4$ cathode

Fig. 4 shows the surface height map of the unaged and aged $LiFePO_4$ cathode samples obtained simultaneously with the surface potential maps. The particles in the unaged sample are more distinct as compared to the particles in the aged sample. The particles are seen to coarsen during the aging of the cells, and thus the surface height image of the aged sample shows increased particle size.

The surface potential maps of the unaged and aged $LiFePO_4$ cathode samples are shown in Fig. 5. The maps were collected by applying +1.0 and +3.3 V from the external DC voltage source. Maps for samples without an externally applied voltage are shown for comparison. Within each surface potential map for both the unaged and aged sample, we observe no large difference in the contrast, suggesting an almost uniform dissipation of charge over the surface of the samples under the externally applied voltage. This indicates that under the external source the sample tends to charge uniformly even in an aged condition. The uniform charging is good for the cell as it avoids large local currents and subsequent damage to the cathode.

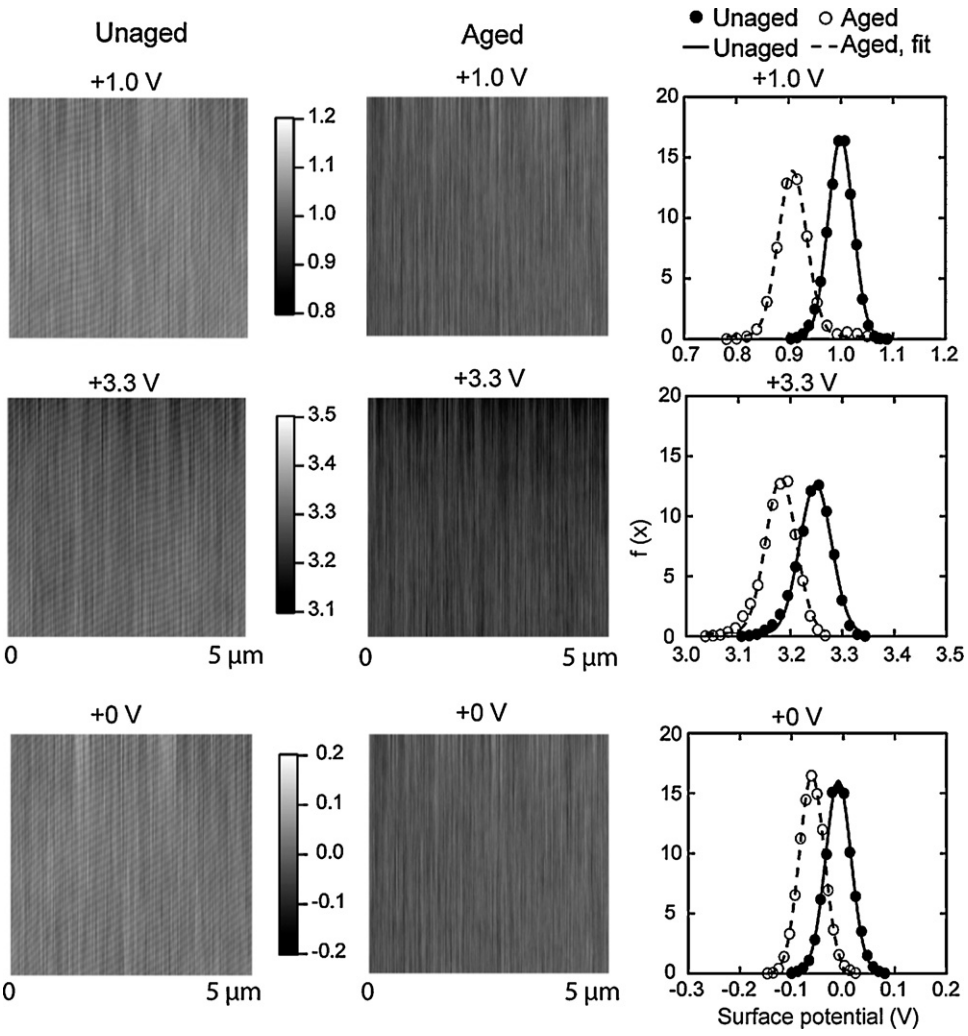

Fig. 5. Surface potential map of the unaged (left column) and the aged (middle column) $LiFePO_4$ cathode samples with external voltage of +1 and +3.3 V. The data for sample without any external voltage is shown for comparison. The right column shows the normal probability density distribution of the surface potential values obtained for the unaged and aged samples. The mean value of the surface potential decreases after aging.

The surface potential image discussed above is generated by a matrix of 256×256 data points. The last column of Fig. 5 also shows the distribution of these data points in unaged and aged cathodes. For each case a histogram is created with 17 equally spaced bins. The bin size was optimized using Sturges's rule [13]:

$$k = 1 + \log_2(n) \tag{4}$$

where k is the number of bins, and n is total number of data points. Then a normal probability density function as shown below is used to fit the data [3]:

$$f(x) = \frac{1}{\sqrt{2\pi\sigma^2}} e^{-((x-\mu)^2/2\sigma^2)} \tag{5}$$

where μ is the mean, and σ is the standard deviation of the data points. The unaged sample had mean values of the surface potential almost equivalent to the external applied voltage. The mean values of surface potential on the aged sample are lower than that of the unaged sample. Thus, even though the externally applied voltage was the same for the unaged and aged samples the charge sustained on the surface of the aged cathode is less than that sustained on the unaged cathode.

The surface potential measured using KPM is the difference between the work functions of the tip and sample surface. Since the same kind of tip is used in these experiments, the work function of the tip is constant in each surface potential map. Fig. 5 shows the change in the work function of the aged sample as compared to the unaged sample. The work function is the property of the structure near the surface of the sample along with the chemical potential of the surface. The decreased surface potential in the aged sample is the indication of the surface modification and could occur due to one or all of the factors discussed below.

A phase change of the cathode material occurs from $LiFePO_4$ to $FePO_4$ and back to $LiFePO_4$ during respective charging and discharging cycles of the battery. During charging, the Li ions from the $LiFePO_4$ cathode are intercalated in the graphite anode. During discharging, the Li ions move out of the graphite anode and are intercalated back in the cathode. The olivine structured $LiFePO_4$ has a different work function that of the metastable $FePO_4$. The change in the surface potential map of the aged sample indicates that one of the phases might be growing in the cathode sample during the battery aging. Andersson and Thomas [2] have demonstrated this phase change as a source of initial capacity loss using neutron diffraction data. Based on their experiments they have proposed a radial model and a mosaic model for the phase change between $LiFePO_4$ and $FePO_4$. In either of their models they have suggested unconverted inactive regions of $LiFePO_4$ entrapped by the $FePO_4$ phase. They concluded that, in reality the superposition of the essential features of the two models might be occurring.

As can been seen in the surface height map (Fig. 4), and also in our previous studies the particles tend to coarsen in the aged sam-

ple as compared to the unaged sample [11]. Due to this coarsening of the nanoparticles and other electrochemical reactions, there is a loss of the conductive carbon coating over the age of the battery. Thus, the large particle size along with the loss of the conductive carbon coating alters the surface electrical properties of the aged sample. Thus, several factors affect the surface potential map of the aged cathode samples.

4. Conclusion

Surface potential was measured under external voltages of +1.0 and +3.3 V in unaged and aged $LiFePO_4$ cathode samples. The surface potential distribution in KPM indicated a larger charge sustaining capacity in the unaged sample compared to aged sample under the same externally applied voltage. The change in the surface potential is attributed to phase change, nanoparticle coarsening and loss of carbon coating. As KPM has high sensitivity to the effects of structural and/or chemical changes, the ability to scan relatively large areas, and locating the modified surfaces, it can be instrumental to detecting the damage mechanism of the cathode sample even before structural and chemical changes in the $LiFePO_4$ cathode can be observed with any other technique. Thus, a KPM study of a $LiFePO_4$ cathode extracted from batteries aged to different degrees of life would provide information about the onset of damage and a relationship between the surface modifications and the age of the battery.

Acknowledgments

The authors sincerely thank Institute for Materials Research (IMR) at The Ohio State University for providing the financial support for this research. The authors are very grateful to Tim Frech from Edison Welding Institute for his help with the setup of the demonstration sample. Authors would like to thank Usama Heiba and Dr. Manuel Palacio for providing assistance with experimental setup.

References

[1] Anonymous, USABC Goals for Advanced Batteries for EVs, USABC, Southfield, MI, 2006, http://www.uscar.org/guest/view_team.php?teams_id=12.
[2] A.S. Andersson, J.O. Thomas, J. Power Sources 97–98 (2001) 498–502.
[3] J.S. Bendat, Piersol, Engineering Applications of Correlation and Spectral Analysis, second ed., Wiley, New York, 1986.
[4] C. Benoit, S. Franger, J. Solid State Electrochem. 12 (2008) 987–993.
[5] B. Bhushan, Nanotribology and Nanomechanics—An Introduction, second ed., Springer-Verlag, Heidelberg, Germany, 2008.
[6] B. Bhushan, A. Goldade, Appl. Surf. Sci. 157 (2000) 373–381.
[7] D. DeVecchio, B. Bhushan, Rev. Sci. Instrum. 60 (1998) 3618–3624.
[8] J.B. Goodenough, J. Power Sources 174 (2007) 996–1000.
[9] S.C. Nagpure, B. Bhushan, in: B. Bhushan, H. Fuchs (Eds.), Applied Scanning Probe Microscope Methods—Biomimetics and Industrial Applications, vol. 13, Springer-Verlag, Heidelberg, Germany, 2009, pp. 203–233.
[10] S.C. Nagpure, B. Bhushan, S.S. Babu, G. Rizzoni, Scripta Mater. 60 (2009) 933–936.
[11] S.C. Nagpure, R. Dinwiddie, S.S. Babu, G. Rizzoni, B. Bhushan, T. Frech, J. Power Sources 195 (2010) 872–876.
[12] A. Rice, Nanoscope Controller Manual, Rev. B, Veeco Instruments, Inc., Santa Barbara, CA, 2002.
[13] H.A. Sturges, J. Am. Stat. Assoc. 21 (1926) 65–66.
[14] A.L. Zharin, D.A. Rigney, Tribol. Lett. 4 (1998) 205–213.